

AN EXPERIMENTAL ASSESSMENT OF THE IMAGING QUALITY  
OF THE LOW ENERGY GAMMA-RAY TELESCOPE ZEBRA.

Butler, R.C., Caroli, E., Di Cocco, G., Natalucci, L.  
Spada, G., Spizzichino, A. and Stephen, J.B.  
Istituto TESRE - CNR, Via De' Castagnoli 1,  
40126 Bologna, ITALY.

Carter, J.N., Charalambous, P.M., Dean, A.J., Graeme, G.,  
Maggioli, P., Young, N.G.S. and Younis, F.  
Physics Department, Southampton University,  
Highfield, Southampton, UK.

Boella, G., Perotti, F. and Villa, G.  
Istituto di Fisica Cosmica, Milan, ITALY.

La Padula, C., Ubertini, P.  
Istituto Astrofisica Spaziali, Frascati, ITALY.

ABSTRACT

One gamma-ray detection plane of the ZEBRA telescope, consisting of nine position sensitive scintillation crystal bars designed to operate over the spectral range 0.2 to 10 MeV, has been constructed in the laboratory. A series of experimental images has been generated using a scaled down flight pattern mask in conjunction with a diverging gamma-ray beam. Point and extended sources have been imaged in order to assess quantitatively the performance of the system.

1. INTRODUCTION. The balloon-borne low energy gamma-ray imaging telescope ZEBRA is designed to operate in the spectral range 0.2 - 10 MeV. A detailed description of the telescope configuration may be found elsewhere (1). It consists of two independent detection modules mounted on either side of a three axis gimbal system. Each module comprises a position sensitive detection plane (PSD) of 9 Sodium Iodide scintillation bars, each of dimensions 5.8cm x 5.0cm x 55cm, with 13 similarly sized non position sensitive bars for anticoincidence purposes. At a distance of 3.5 metres in front of this plane is situated a coded aperture mask, constructed out of Tungsten alloy elements arranged in a 2 x 2 mosaic of a 9 x 7 Uniformly Redundant Array (URA) pattern (2). The intrinsic angular resolution of the device is governed by the angle subtended by a mask element at the detection plane. For the ZEBRA telescope this amounts to

$\sim 1^\circ \times \sim 1^\circ$ . The point source location accuracy, however, is determined by the positional resolution of the detection plane and the strength of the detected source. For this reason, the bars in either detection module are mounted orthogonally in order to symmetrise and optimise this parameter.

The position sensitive detection bars have been studied carefully in the laboratory environment in order to fully assess their imaging capabilities. The initial tests were performed on single bar imaging systems (3), extending later to experimental systems of several bars operating in conjunction to provide two dimensional data.

In the last few months, a full ZEBRA PSD of nine bar units has been assembled in the laboratory and a series of experimental images has been generated. The arrangement consisted of the 9 bar plane in front of which, at a distance of 2.5 metres, a half-size 9 x 7 pattern mask was aligned so as to be perfectly parallel. This configuration naturally leads to the imaging system being 'focussed' on a source plane a further 2.5 metres from the PSD. Signals from the 18 photomultiplier tubes were digitised by two ADC's and stored on magnetic tape via a PDP 11/24 computer, subsequent analysis being performed on an HP 1000 computing system.

Two types of source distribution were studied: point sources, both single and multiple, and extended sources artificially contrived by continuously moving a point source during the integration period. For these laboratory experiments a preliminary calibration of the detection plane was performed by means of a collimated source (Cs.137  $\sim 662$  keV) placed very close to each bar in succession at three well determined positions along the length. An energy look-up table was also calculated for each bar in order to provide a uniform spectral response both down the length of the bars and between the entire set.

## 2. EXPERIMENTAL IMAGES.

a) Point Sources. A 100  $\mu$ C Cs 137 source was employed as the object to be imaged. At a distance of  $\sim 5$  metres the counting rate was found to be  $\sim 15\%$  of the integrated background event rate. The source was placed in over 80 well defined positions across the object plane and images accumulated for  $10^{**}5$  events (i.e. about  $1.5 \times 10^{**}4$  source counts). For the purposes of analysis, an energy window around 662 keV was established such that only events under the Cs energy loss photopeak were accepted.

The data were binned in 128 energy bins of which 112 corresponded to the active region of the bars (the central 49cm), thus the shadow of one mask element covered 16 pixels. A straightforward correlation analysis (4) of the 9

x 112 data set and the 9 x 7 mask pattern allowed reconstruction of the source distribution. A typical example of the many images obtained is shown in Figure 1.

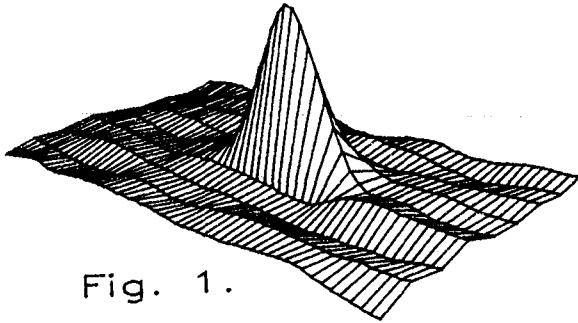


Fig. 1.

The triangular point spread function intrinsic to this decoding method is readily apparent. In this image there are  $\sim 5 \times 10^4$  source counts and  $\sim 3 \times 10^4$  background events. The full width at half maximum of the peak is  $16.45 \pm 0.13$  channels in comparison to the theoretical minimum

of 16. The larger figure is due to the finite positional resolution of the detection plane and mechanical errors in setting up the experiment.

Figure 2. shows the reconstructed peak positions obtained from 6 images in comparison to the true source positions, the data being expressed in arcminutes from the centre of the field of view. The line is a weighted least squares fit to the experimental data. The error bars are 1 sigma, and it can be seen that the two sets of data are in excellent agreement.

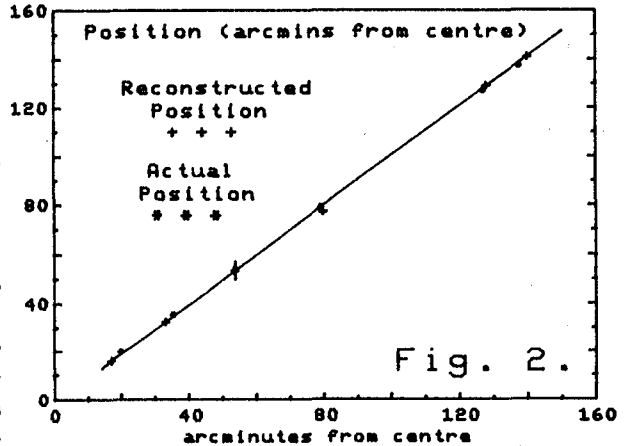


Fig. 2.

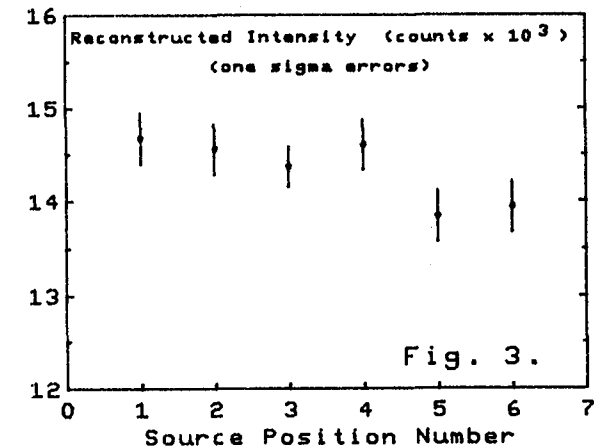


Fig. 3.

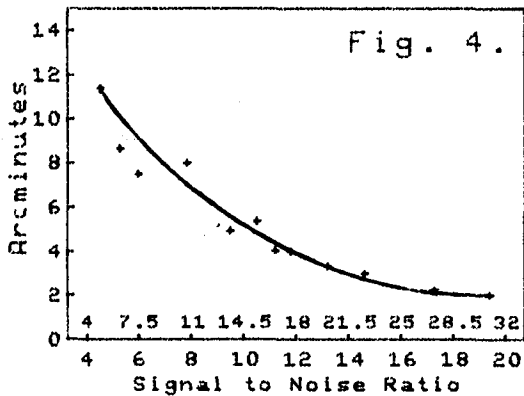
a combination of the cosine effect, self vignetting by the body of the mask and the reduced apparent integral thickness of the detection plane (5,6).

A slight magnification mismatch is evident, probably due to difficulties in employing a diverging gamma-ray beam and the subsequent need to measure mask/source and mask/PSD distances very accurately.

The reconstructed intensity at each position is shown in Figure 3. Some very slight reduction in intensity for more off-axis sources is apparent. This is due to

The point source location accuracy as a function of signal to noise ratio (SNR) is depicted in Figure 4. The two scales on the X-axis reflect the different values which

may be attributed to the variance of the background, either with or without accounting for systematic structure.



b) Extended Sources. In order to simulate an extended source, a point source was made to rotate within the field of view. Several images were accumulated for different radii. Figure five depicts such a source with a radius of 20 cm ( $\sim 2^\circ$ ). The centre of the distribution falls to the background level as

expected. Analysis of the extended source distributions is continuing.

**3. CONCLUSIONS** This paper presents the first two dimensional images to be obtained using one full ZEBRA detection PSD. Using only preliminary laboratory calibration procedures, and making no allowance for non-uniformities in the background event rate (such as background subtraction) it has been demonstrated that high quality images may be obtained. The point source location accuracy is at the arc minute level.

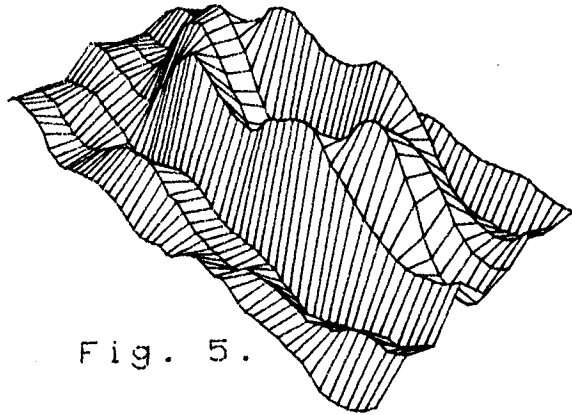


Fig. 5.

#### REFERENCES

1. Baker, R.E. et al Proceedings 18th ICRC, Bangalore (1983)
2. MacWilliams, F.J. and Sloane, N.J.A. Proc. IEEE 64 1715 (1976)
3. Charalambous, P.M. et al Nucl. Instr. and Meths. in Phys. Res. 221 183 (1984)
4. Fenimore, E.E. and Cannon, T.M. Appl. Opt. 17 337 (1978)
5. Butler, R.C. et al Nucl. Instr. and Meths. in Phys. Res. 221 41 (1984)
6. Charalambous, P.M. et al Appl. Opt. 23 4118 (1984)